

# Role of ATM in the telomere response to the G-quadruplex ligand 360A

Gaëlle Pennarun<sup>1</sup>, Christine Granotier<sup>1</sup>, Françoise Hoffschir<sup>1</sup>, Eliane Mandine<sup>2</sup>, Denis Biard<sup>3</sup>, Laurent R. Gauthier<sup>1</sup> and François D. Boussin<sup>1,\*</sup>

<sup>1</sup>CEA, DSV, IRCM, Laboratoire de Radiopathologie-IPSC, 92265 Fontenay-aux-Roses, <sup>2</sup>Aventis Pharma SA, Centre de Recherche de Paris, 94403 Vitry-sur-Seine and <sup>3</sup>CEA, DSV, IRCM, Laboratoire de Génétique de la Radiosensibilité, 92265 Fontenay-aux-Roses, France

Received October 29, 2007; Revised and Accepted January 16, 2008

## ABSTRACT

**Telomeres are known to prevent chromosome ends from being recognized as DNA double-strand breaks. Conversely, many DNA damage response proteins, including ATM, are thought to participate to telomere maintenance. However, the precise roles of ATM at telomeres remain unclear due to its multiple functions in cell checkpoints and apoptosis. To gain more insights into the role of ATM in telomere maintenance, we determined the effects of the G-quadruplex ligand 360A in various cell lines lacking functional ATM. We showed, by using Fluorescence *in situ* hybridization (FISH) and Chromosome Orientation-FISH using telomere PNA probes, that 360A induced specific telomere aberrations occurring during or after replication, mainly consisting in sister telomere fusions and also recombinations that involved preferentially the lagging strand telomeres. We demonstrate that ATM reduced telomere instability independently of apoptosis induction. Our results suggest thus that ATM has a direct role in preventing inappropriate DNA repair at telomeres, which could be related to its possible participation to the formation of protected structures at telomeres.**

## INTRODUCTION

Human telomeric DNA contains double-stranded repeats of the motif TTAGGG followed by a G-rich 3'-overhang and is capped by a specific telomere multiprotein complex referred to as shelterin (1). Telomeres can adopt a protective T-loop structure in which the telomeric 3'-overhang is incorporated into the proximal double-stranded telomeres (2). T-loop has been proposed to

prevent telomeres from being recognized as DNA double-strand breaks (DSBs) and thus from activating cell cycle checkpoints, inappropriate DNA repair and cell death.

The ATM (ataxia telangiectasia mutated) gene product is involved in the rare disease ataxia-telangiectasia (AT) characterized by progressive cerebellar degeneration, immunodeficiency and cancer predisposition. AT cells exhibit abnormalities including defects in cell cycle checkpoints, increased radiation sensitivity and chromosome instability. ATM belongs to the phosphoinositol 3-kinase family and plays crucial roles in cellular response to DNA damage (3–5). ATM is principally activated following DNA DSBs throughout the cell cycle by autophosphorylation of its residue serine 1981 (6,7) and leads to the phosphorylation of multiple downstream proteins principally involved in DNA damage recognition, cell cycle checkpoints and apoptosis (8), such as p53, H2AX, CHK2 and SMC1.

ATM has been reported to be the main transducer of the telomere damage signal due to telomere attrition during senescence or TRF2 (telomeric repeat factor 2) inhibition (9,10). TRF2 was reported to be a specific inhibitor of ATM on telomeres (9–11). It has been demonstrated that mutations in ATM lead to defective telomere maintenance in mammalian cells (3). Indeed, AT cells show increase chromosome end-to-end association and telomere loss. Particularly AT cells are more prone to telomere fusion after irradiation than normal cells (3,12,13). ATM influences the interactions between telomeres and the nuclear matrix, and alterations in telomere chromatin could be at least partly responsible for the pleiotropic phenotypes of the ATM gene defect (14). This is illustrated by the accumulation of cells with clustered telomeres during meiosis in ATM null cells, which account for infertility (15). Recent reports have also shown that ATM was recruited at telomeres in G2 phase of the cell cycle and it has been suggested that telomere ends need to be recognized as DNA damage to complete

\*To whom correspondence should be addressed. Tel: +33 1 46 54 97 91; Fax: +33 1 46 54 97 02; Email: boussin@cea.fr

The authors wish it to be known that, in their opinion, the first two authors should be regarded as joint First Authors.

© 2008 The Author(s)

This is an Open Access article distributed under the terms of the Creative Commons Attribution Non-Commercial License (<http://creativecommons.org/licenses/by-nc/2.0/uk/>) which permits unrestricted non-commercial use, distribution, and reproduction in any medium, provided the original work is properly cited.

end replication and to acquire a structure that is essential for function (16–18). However, the exact roles of ATM at telomeres remained largely unclear due to its multiple functions. It is particularly difficult to discern a possible role in telomere replication from its role at dysfunctional telomeres and in induction of cell checkpoints and apoptosis.

Structure studies (X-ray crystallography and nuclear magnetic resonance) of oligonucleotides have indicated that the telomeric-3'-overhang could adopt a variety of quadruplex structures based on four Hoogsteen-paired, coplanar guanines (19–21), referred to as G-quadruplex. Various G-quadruplex ligands have been described to have antiproliferative effects toward cancer cells (22,23). We have previously identified a highly selective G-quadruplex ligand 360A (24), a 2,6-pyridine-dicarboxylate derivative that can bind to human chromosome end *in vivo* (25) and provokes telomere instability and apoptosis in immortalized cell lines (24).

Here, we compare the effects of the G-quadruplex ligand 360A on various ATM-deficient or knocked-down cells lines. We provide evidences that ATM has a direct role in preventing inappropriate DNA repair at dysfunctional telomeres independently of cell cycle checkpoint and apoptosis induction.

## MATERIALS AND METHODS

### Chemical compounds

360A is a 2,6-pyridine-dicarboxamide derivative displaying strong affinity and selectivity for G-quadruplex structures and selective telomerase inhibition in *in vitro* assays (24). 360A was dissolved at 10 mM in dimethyl sulfoxide (DMSO), stored at  $-20^{\circ}\text{C}$  and diluted with culture medium immediately before use.

### Cell culture

Stable knockdown HeLa clones for ATM gene (ATM<sup>KD</sup>) expressing small interfering RNA (siRNA) have been previously described [(26,27) and Supplementary Figure 1). As control, we used a stable HeLa clone transfected with a control EBV vector (pBD650) (26). HeLa clones ( $1 \times 10^6$  cells/flask) were cultured in DMEM medium supplemented with 10% Fetal Bovine Serum (FBS, ATGC), 2 mM glutamine, antibiotics (penicillin, 200 U/ml and streptomycin, 200  $\mu\text{g}/\text{ml}$ , Sigma), 1 mM HEPES (Invitrogen) and 250  $\mu\text{g}/\text{ml}$  hygromycin B (Invitrogen). Simian virus 40 (SV40)-transformed human normal fibroblast (AS3WT2) (28) and SV40-transformed AT fibroblast (GM09607) cell lines ( $1 \times 10^6$  cells/flask) were cultured in DMEM medium with 10% FBS, glutamine and antibiotics. EBV-transformed lymphocyte cell lines derived from normal (GM03657) and AT donors (GM03189, Coriell Cell Repositories) were cultured at  $3\text{--}5 \times 10^5$  cells/ml in RPMI medium (Sigma) with 15% FBS, glutamine and antibiotics.

Cells were cultured with 5  $\mu\text{M}$  360A, a concentration at which we have previously shown that 360A induced a strong telomere instability (24), or with the corresponding concentration of DMSO (0.05%) as controls.  $\gamma$ -irradiated

cells (IBL637, CisBio International) were collected 1 h after irradiation.

### Cell cycle analysis and apoptosis detection

Cell cycle analysis and quantification of apoptotic cells by TUNEL assays were performed as previously described (24).

### Fluorescent *in situ* hybridization (FISH) and Immuno-FISH

Metaphase spreads were performed as previously described (29), fixed in 4% formaldehyde and hybridized with a telomeric Cyanine-3-conjugated ( $\text{C}_3\text{AT}_2$ )<sub>3</sub> peptide nucleic acid (PNA) probe (Applied Biosystems) complementary to the G-rich telomeric strand using standard PNA-FISH procedures (30) following by hybridization with a FITC-pan-centromeric DNA probe (Cambio). The chromosome preparations were counterstained with DAPI and observed under a fluorescence microscope (Olympus IX81). Image acquisition (coolsnap HQ camera, Princeton instrument) was controlled through MetaMorph software (Universal Imaging): three gray-scales 16-bit images [Dapi, Cyanine 3 (telomere probe) and FITC (centromeres)] with pixel size of 0.13  $\mu\text{m}$  were obtained per metaphase. Then, merging images were created by false-color image superpositions and compressed in 8-bit tiff files. Statistical analyses (*t*-tests) were done with StatView software.

For Immuno-FISH, immunostaining of 53BP1 was performed as described below and followed by incubation in PBS 0.1% Triton X-100, fixation 5 min in 2% paraformaldehyde (PFA), dehydration with ethanol and air dried. Cells were then hybridized with the telomeric FITC-conjugated ( $\text{C}_3\text{AT}_2$ )<sub>3</sub> PNA probe as described above. We calculated the percentage of colocalization of 53BP1 and PNA signals using the module of colocalization of MetaMorph software. 53BP1 was chosen for these experiments since its detection is easier than that of ATM and because 53BP1 foci are less diffuse than that of  $\gamma$ -H2AX increasing the stringency of the analysis.

### Chromosome orientation-FISH (CO-FISH)

CO-FISH allows to differentiate chromosome lagging strand telomeres from leading strand telomeres by the respective detection of parental TTAGGG and CCCTAA telomere strands after selective degradation of the neosynthesized strands. CO-FISH was performed as previously described (31,32) with few modifications. Briefly, cells were grown in complete medium containing BrdU (10  $\mu\text{M}$ ) for one cell cycle. Metaphase spreads were performed as described above. Slides were treated with RNase (0.5 mg/ml), stained with Hoechst 33258, exposed to UV light and digested with exonuclease III. After dehydration, slides were hybridized (2 h at RT) with a telomeric FITC-conjugated ( $\text{T}_2\text{AG}_3$ )<sub>3</sub> PNA probe (Applied Biosystems) complementary to the C-rich telomeric strand (leading strand), following by an incubation (2 h at RT) with a telomeric Cyanine-3-conjugated ( $\text{C}_3\text{AT}_2$ )<sub>3</sub> PNA probe complementary to the G-rich telomeric strand (lagging strand). After washings and

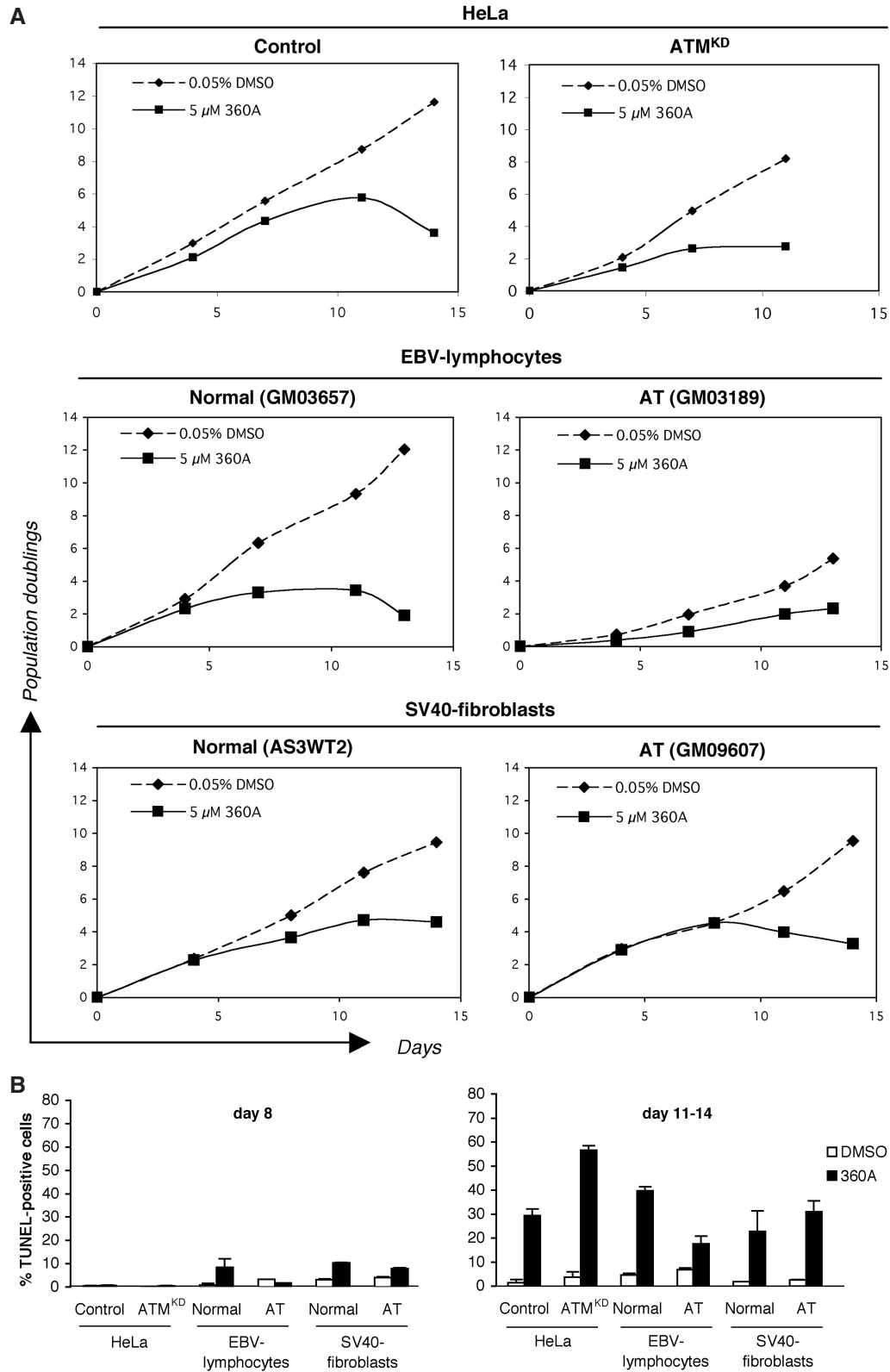


**Figure 1.** Cell growth arrest and apoptosis induced by the G-quadruplex ligand 360A in ATM-proficient and deficient immortalized cell lines. **(A)** Cell growth curves of ATM<sup>KD</sup> and control HeLa cells, normal (GM03657) and AT (GM03189) EBV-lymphocytes, and, normal (AS3WT2) and AT (GM9607) SV40-fibroblasts treated with 5 μM 360A or 0.05% DMSO as controls. 360A induced cell growth arrest following by massive cell death in all these cell lines. Similar results were obtained at least in three independent experiments. **(B)** TUNEL labeling of cells treated with 5 μM 360A (or 0.05% DMSO) for 8 days (on the left) or for longer times (11 days or 14 days for SV40-fibroblasts) (on the right). Samples were analyzed by flow cytometry and the proportion of TUNEL-positive cells was expressed as percentage of total population. Data are the means ± SE of at least two independent experiments.

DAPI counterstained, at least 30 metaphases per condition were scored.

### Immunostaining

The sources of primary antibodies were as follows: mouse anti- $\gamma$ -H2AX clone JBW301 and mouse anti-ATM phosphoserine 1981 clone 10H11.E12 (Upstate); rabbit anti-SMC1 phosphoserine 957 and rabbit anti-53BP1 (Novus Biologicals); rabbit anti-ATM phosphoserine 1981 (Abcam).

After a blocking step (10% FBS in PBS or 3% BSA in 0.1% Triton X-100 TBS, 1 h at RT), cells previously fixed (either in 50% methanol/50% acetone, 1 h at  $-20^{\circ}\text{C}$  or 95% ethanol/5% acetic acid, 5 min at RT or 4% PFA for 10 min followed by permeabilization in 0.1% Triton X-100 PBS), cells were incubated with the primary antibody in blocking buffer (1 h at RT or overnight at  $4^{\circ}\text{C}$ ), then washed and incubated with Alexa-conjugated secondary antibody (Molecular Probes) for 1 h. Cells were counterstained with DAPI before observation under a fluorescence microscope (Olympus B51). For each condition, 50 to 200 random chosen cells were counted. Statistical analyses were done with StatView software (Abacus Concepts).

## RESULTS

### ATM attenuates 360A-induced telomere instability

We have previously shown that the pyridine derivative G-quadruplex ligand 360A induced telomere instability and cell death in various cell lines (24). In order to evaluate the importance of ATM for telomere maintenance, we tested the effects of 360A in stable HeLa cells expressing siRNA knocking down ATM (ATM<sup>KD</sup> HeLa cells) (27) and control HeLa cells (carrying a pEBV-based plasmid with an inactive siRNA), which allowed us to determine the consequences of ATM defect in a same cellular context. We also treated cell lines derived from AT patients [ATM-deficient EBV-lymphocyte (GM03189) and SV40-fibroblast (GM09607) cell lines] and their respective ATM-proficient controls prepared from normal donors.

ATM-deficient cells have been shown to be hypersensitive to ionizing radiation and radiomimetic drugs (3). However, 360A induced decrease in population doublings followed by apoptotic cell death within 14 days of treatment in all ATM-deficient and proficient cell lines as in ATM<sup>KD</sup> HeLa cells and controls (Figure 1).

We then analyzed the chromosome aberrations induced by 360A on metaphase spreads after 8 days of treatment, thus before induction of significant cell death (Figure 1B). Contrary to genotoxic stresses such as ionizing radiation, 360A neither modified significantly the average numbers of chromosomes per cell, nor induced chromatid breaks in the cell lines studied whatever their ATM status (data not shown and Supplementary Figure 2). However, FISH with telomeric and centromeric probes on metaphase spreads showed that 360A induced a strong telomere instability leading to a broad spectrum of telomere aberrations with  $16.7\% \pm 0.9$  chromosomes with damaged

telomeres in 360A-treated HeLa cells versus  $7.3\% \pm 0.4$  in untreated controls (t-test  $P$ -value  $<0.0001$ ). Telomere damages were significantly more abundant (t-test  $P$ -value  $<0.0001$ ) in 360A-treated ATM<sup>KD</sup> HeLa cells with  $32.6\% \pm 1.8$  chromosomes with damaged telomeres versus  $11.6\% \pm 1.0$  in control cells (Figure 2).

360A induced the formation of dicentric chromosomes resulting from telomere fusion—as deduced from the presence of telomeric signals at the fusion points—in similar range than that reported for other G-quadruplex ligands (24,33,34). By contrast 360A did not induce the formation of dicentric chromosomes lacking telomere sequences at the fusion points suggesting the specific involvement of telomere destabilization in chromosome fusions induced by 360A (Supplementary Figure 3). Interestingly, we showed that 360A induced more sister telomere fusions than telomere fusions of two distinct chromosomes (Figure 2). 360A also induced telomere aberrations previously described in other models in which telomeres were destabilized: telomere losses—as shown by chromosomes lacking telomere signal on one or two sister chromatids (referred to as one telomere loss and terminal deletion, respectively)—extrachromosomal telomere signals—that could not be quantified precisely—(35), telomere doublets at single chromatid ends (13,36) and telomeric DNA-containing double minute chromosome (TDM) (37) (Figure 2).

Similar results were obtained with EBV-lymphocyte and SV40 fibroblast cell lines, in which FISH also showed that 360A increased telomere aberrations in a greater extent in AT cells compared to ATM-proficient cells (Supplementary Figure 4).

Consistent with a role of ATM in telomere maintenance, we found a significant increase in spontaneous telomere aberrations in ATM-knockdown and ATM-deficient cell lines compared to their controls with 1.4–2% more of damaged telomeres in each cell lines studied (Figure 3). In order to ascertain that ATM has also a role in the response to 360A, we compared the percentages of telomere aberrations directly attributable to 360A in each cell lines that we estimated by subtracting the background telomere instability—calculated from DMSO controls (Table 1)—from the percentages of total damaged telomeres found in 360A-treated cells. Table 1 shows that ATM defect significantly increased (1.8–2.4 times, t-test  $P$ -value  $\leq 0.0005$ ) telomere damages induced by 360A in the three different cellular contexts studied.

Altogether these results confirmed that treatment with 360A induced a massive cell death of immortalized cell lines after few population doublings associated with the induction of telomere instability and that ATM deficiency significantly increased telomere damages induced by 360A.

### Increases in telomere aberrations in 360A-treated ATM deficient or knocked-down cells are not related to defects in cell cycle checkpoint and apoptosis induction

Induction of cell cycle checkpoints and apoptosis are generally considered to be essential functions of ATM signaling following DNA damages (4,8,38).

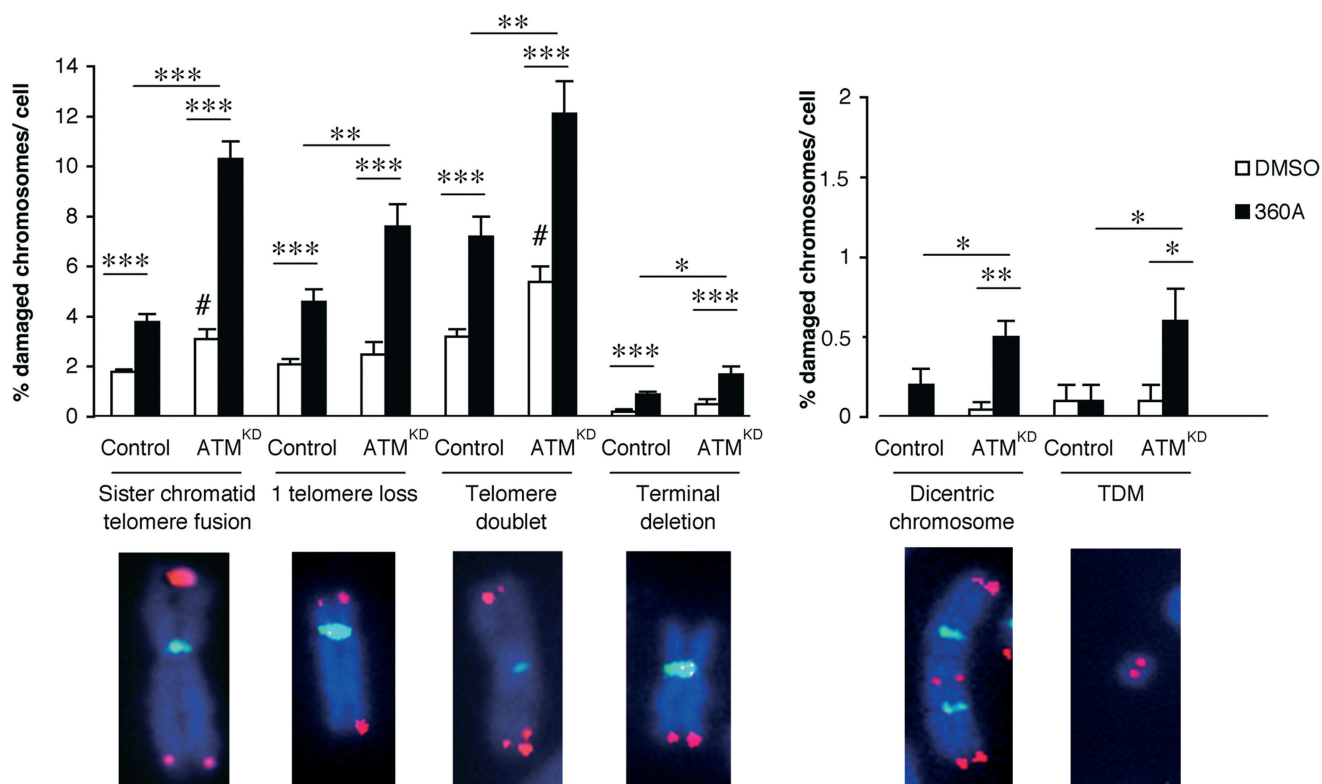


**Figure 2.** 360A induces specific telomere aberrations in HeLa cells that are increased in ATM knocked down cells. Histograms show the percentages of chromosomes with the indicated telomere aberration per cell detected in metaphase spreads of ATM<sup>KD</sup> and control HeLa cells treated with 5  $\mu$ M 360A for 8 days (or 0.05% DMSO) and hybridized successively with a telomeric PNA probe (in red) and a centromeric DNA probe (in green) and then counterstained with DAPI (blue). Percentages  $\pm$  SEs were calculated from  $n = 30$  metaphases per condition. The mean number of chromosomes per cell was 66 and remained unchanged in ATM<sup>KD</sup> and control HeLa cells. \*Indicates a  $t$ -test  $P$ -value  $\leq 0.05$ ; \*\* $P < 0.001$ ; \*\*\* $P < 0.0001$ ; #indicates a significant difference between DMSO-treated ATM<sup>KD</sup> and control HeLa cells. Dicentric chromosomes taken into account contained telomere signals at the fused points (No dicentric chromosome without telomere signals at the fused points were detected, see Supplementary Figure 3). Representative images of the different telomere aberrations are presented at the bottom.

Although metaphase analyses have been performed before induction of apoptosis in 360A-treated cultures (Figure 1B), one could speculate that the increase of telomere rearrangements induced by 360A in cells lacking functional ATM was the direct consequence of a defect in cell-cycle checkpoints and apoptosis induction, allowing cells with damaged telomeres to be analyzed at metaphase, contrary to cells with functional ATM.

We thus investigated the effects of ATM on cell cycle progression in 360A-treated cells (Table 2). We found a S-phase accumulation in ATM-proficient, but not in ATM-deficient EBV-lymphocytes treated with 360A before induction of cell death. However, ATM status did not modify cell cycle distribution in 360A-treated SV40-fibroblasts and HeLa cells compared to DMSO-treated controls. This suggests that the lower levels of telomere aberrations found in metaphases of ATM-proficient SV40-fibroblasts and HeLa cells were not due to cell-cycle checkpoint arrest, which would have prevented the analysis of cells with high levels of damaged telomeres.

We then analyzed the distribution of telomere damages in treated cells in function of their ATM status. If ATM deficiency had increased 360A-induced telomere aberrations because of defects in checkpoints activation

and induction of apoptosis of damaged cells, 360A-treated cultures of ATM-deficient cells would have contained a subpopulation of cells with higher percentages of damaged telomeres corresponding to the cells that had escaped checkpoints or death due to the lack of functional ATM. The results (Figure 3) show that this was not the case. First, 360A increased the percentages of telomere aberrations in all normal and ATM-deficient cells. Second, most if not all 360A-treated ATM-deficient cells have a percentage of damaged telomeres largely higher than that found in untreated controls and 360A-treated ATM-proficient cells.

All together our results rule out the hypothesis that the increase of telomere aberrations found at metaphase in ATM-deficient cells was simply the consequence of defects in cell checkpoint activation and apoptosis induction demonstrating thus that ATM has a more direct protective role at telomeres.

### 360A specifically increases sister telomere fusions in ATM<sup>KD</sup> HeLa cells, but does not induce telomere sister chromatid exchange (T-SCE)

We next performed CO-FISH on metaphase chromosomes from ATM<sup>KD</sup> and control HeLa cells treated with

360A (Figure 4) to better characterize the mechanisms leading to telomere instability by determination of the respective involvements of lagging and leading strand telomeres in recombination events or losses.

We first checked for induction of T-SCE by 360A. T-SCE occurs at late S phase or G2 between telomeres of

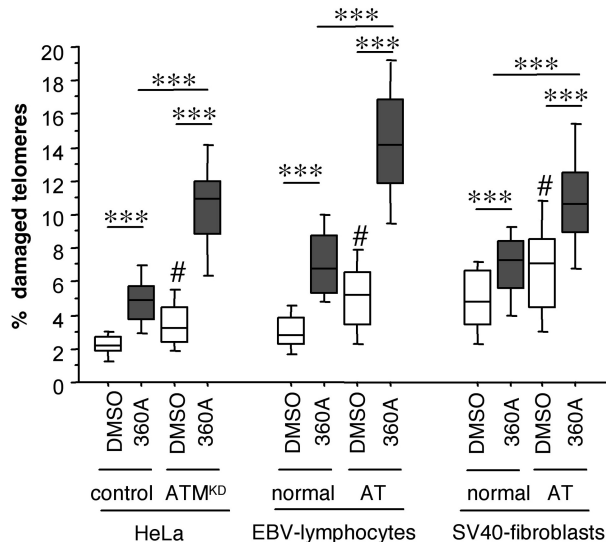


**Figure 3.** The increase of telomere damages concerns all metaphasic cells in 360A-treated ATM-deficient cell cultures. Analysis of the distribution of telomere damages in metaphases from ATM<sup>KD</sup> and control HeLa cells, normal (GM03657) and AT (GM03189) EBV-lymphocytes, and, normal (AS3WT2) and AT (GM09607) SV40-fibroblasts treated with 5  $\mu$ M 360A or 0.05% DMSO for 8 days. Box graph shows the distribution of the percentages of damaged telomeres found in each cell (30 to 80 cells per conditions). Boxes include 50% of the values centered on the median (the horizontal line through the box). The vertical lines begin at the 10th percentile and end at the 90th percentile; \*\*\* indicates a *t*-test *P*-value < 0.0001; # indicates a significant difference between ATM-proficient and deficient cells treated with DMSO. Telomere aberrations taken into account were sister chromatid telomere fusions, one telomere losses, telomere doublets, TDM and dicentric chromosomes with telomere signals at fusion points. Terminal deletions were excluded from these analyses since they could also arise from double-strand breaks, although this had no impact on the final results (data not shown).

**Table 1.** Comparison between percentages of damaged telomeres induced by 360A in metaphase spreads of ATM-deficient cells and in their respective ATM-proficient controls

	Percentage of damaged telomeres		Induced by 360A <sup>c</sup>			
	Background Level <sup>a</sup>	Due to ATM defect <sup>b</sup>	ATM-proficient	ATM-deficient	Ratio	<i>t</i> -test <i>P</i> -value
HeLa	2.2 $\pm$ 0.1 ( <i>n</i> = 30)	1.4 $\pm$ 0.3 ( <i>n</i> = 30)	2.7 $\pm$ 0.3 ( <i>n</i> = 30)	6.9 $\pm$ 0.5 ( <i>n</i> = 28)	2.5	< 0.0001
EBV-lymphocytes	3.2 $\pm$ 0.4 ( <i>n</i> = 30)	1.9 $\pm$ 0.4 ( <i>n</i> = 30)	4.0 $\pm$ 0.4 ( <i>n</i> = 30)	9.6 $\pm$ 0.9 ( <i>n</i> = 30)	2.4	< 0.0001
SV40-fibroblasts	4.9 $\pm$ 0.2 ( <i>n</i> = 81)	2.0 $\pm$ 0.3 ( <i>n</i> = 65)	2.2 $\pm$ 0.3 ( <i>n</i> = 55)	3.9 $\pm$ 0.4 ( <i>n</i> = 80)	1.8	0.0005

Ratios were calculated by dividing the values from ATM-deficient cells by those from ATM-proficient cells. The *t*-test *P*-values indicate a significant difference between ATM-deficient and ATM-proficient values.

<sup>a</sup>Percentages of damaged telomeres  $\pm$  SE found in ATM-proficient DMSO controls calculated from *n* cells.

<sup>b</sup>Percentages of damaged telomeres  $\pm$  SE due to ATM deficiency in the different cell contexts were calculated from percentages of damaged telomeres found in DMSO-treated ATM-deficient cells minus the mean of damaged telomeres observed in ATM-proficient DMSO controls.

<sup>c</sup>Percentages of damaged telomeres  $\pm$  SE induced by 360A (5  $\mu$ M for 8 days) in the different cell contexts were calculated from *n* cells minus mean of percentages damaged telomeres determined in the respective DMSO controls.

sister chromatids. In this process, the G-overhang of one telomere invades the other telomere and anneal with complementary sequences acting as a primer for shortening or elongating telomeres when exchanged segments are not equal extension (1). Although none of the cell lines involved in this study are alternative lengthening of telomeres (ALT) cells, in which T-SCE has been shown to occur principally (39), one could not exclude that T-SCE was induced by the G-quadruplex ligand. However, results of CO-FISH demonstrated the lack of exchange between leading and lagging strand telomeres and thus that 360A did not significantly induce T-SCE in HeLa cells whatever their ATM status (Supplementary Table 1).

CO-FISH showed that 360A-induced sister chromatid fusions systematically contained both parental lagging and leading strands at the fusion point in both control and ATM<sup>KD</sup> HeLa cells (Figure 4A). Thus, these results confirm that 360A-induced sister chromatid fusions resulted from telomere fusions of sister telomeres—and not from fusion between telomeres and DNA DSBs elsewhere on the chromosome—and the specificity of their increase found in ATM-deficient cells (Figure 2). Altogether these data confirm that ATM protects destabilized sister telomeres from 360A-induced fusions.

#### ATM reduces telomere losses and doublets, which result from lagging strand telomere dysfunctions induced by 360A

We then analyzed by CO-FISH involvement of lagging and leading strand telomeres in the formation of telomere doublets. Telomere doublets are characterized by two telomere arrays (one in terminal position) separated by various lengths of nontelomeric DNA on one sister chromatid, whereas the other keeps a single telomeric signal in terminal position (Figure 4B). Telomere doublets have been reported in other studies but mechanisms leading to their generation remain unknown (13,36). In both treated and untreated cells whatever their ATM status, CO-FISH showed that telomere doublets were mainly made of either two lagging strand telomere sequences or two leading strand telomere sequences, whereas the telomeres of the others chromatids were

not involved in the recombination process (Figure 4B). This observation indicates that mechanisms of generation of telomere doublets involved in most cases neither duplication of telomere sequences—no telomere doublets would have been detected by CO-FISH, since the protocol involved a degradation of duplicated DNA before hybridization—nor sister chromatid exchange—the telomere doublets detectable by CO-FISH would have been made with both lagging and leading telomeres. Interestingly, we found that telomere doublets induced by the G-quadruplex ligand mainly involved the lagging strand telomeres (Figure 4B).

Importantly, CO-FISH also showed (Figure 4B) a significant increase (Chi-square  $P$ -value  $<0.001$ ) in the proportion of telomere doublets made of lagging strand sequences in 360A-treated ATM<sup>KD</sup> HeLa cells (90%) compared to 360-treated controls (79%). This suggests therefore that the increase in telomere doublets evidenced in 360A-treated ATM knockdown cells (Figure 2) involved preferentially the lagging strand telomeres, indicating thus that ATM specifically protects the lagging strand telomeres from 360A-induced formation of telomere doublets.

We next investigated the chromosomes missing one telomere. CO-FISH demonstrated an increase in the proportion of telomere loss involving the lagging-strand telomere in 360A-treated cells (Figure 4C). This was not due to a weaker sensitivity of the C-probe or competition with the G-quadruplex ligand, since in the same experiments most of extrachromosomal telomere signals (data not shown) and telomere doublets (as shown above) were found to involve the lagging and not the leading strand telomeres. This result indicates that the increase in telomere loss found in 360A-treated cells (Figure 2) resulted from the preferential deletion of the lagging strand telomeres. This demonstrates thus that the mechanism of telomere loss induced by 360A involved specific telomere impairment and was not due to an unrelated cause such as DSBs occurring upstream telomeres.

Moreover, as for telomere doublets, CO-FISH showed a significant increase (Chi-square  $P$ -value  $<0.001$ ) in the proportion loss of the lagging strand telomeres in 360A-treated ATM<sup>KD</sup> cells (85%) compared to 360A-treated HeLa controls (63%) (Figure 4C). Altogether, our results suggest therefore that the compound specifically induced recombination of the lagging strand telomeres resulting either in telomere doublet or telomere loss and that ATM specifically prevents these mechanisms to occur.

Interestingly, CO-FISH also showed that a significant increase (Chi-square  $P$ -value  $<0.001$ ) in the proportion of telomere loss concerning the lagging strand telomeres in untreated ATM<sup>KD</sup> HeLa cells (72%) compared to control HeLa cells (52%) (Figure 4C). This indicates therefore that the increase in telomere loss evidenced in untreated ATM<sup>KD</sup> cells (Figure 2C) involved preferentially the lagging strand telomeres, which significance for ATM putative roles at telomeres during unperturbed replication remains to be further investigated.

### The G-quadruplex ligand 360A induces a DNA damage signaling in a strictly ATM-dependent manner

In order to further investigate the role of ATM in response to 360A, we then studied ATM signaling in HeLa cells. We found that 360A significantly increased nuclear foci of activated ATM by performing immunofluorescence staining with an antibody against its phosphorylated form (serine 1981) (Figure 5A and B). These foci colocalized with that of phosphorylated H2AX, a member of the nucleosome core histone H2A family, which is phosphorylated on serine 139 (referred to as  $\gamma$ -H2AX) mainly by ATM, at chromatin adjacent to DNA DSBs (40) and at dysfunctional telomeres (10,41). 360A induced a significant increase in the number of  $\gamma$ -H2AX nuclear foci in HeLa cells compared to DMSO controls (Figure 5A and B). 360A also induced the formation of nuclear foci of 53BP1 and of the phosphorylated forms of SMC1, which for the most colocalized with that of

**Table 2.** Cell-cycle distribution of ATM-deficient cells and their respective ATM-proficient controls treated for 7–8 days with 5  $\mu$ M 360A or 0.05% DMSO.

Cell line	ATM status	Treatment	Cell-cycle distribution (%) <sup>a</sup>			$\chi^2$ $p$ -values <sup>b</sup>
			G1	S	G2/M	
HeLa	Control	0.05% DMSO	57.3 $\pm$ 0.1	32.6 $\pm$ 0.5	10.1 $\pm$ 0.4	ns
		5 $\mu$ M 360A	57.9 $\pm$ 2.1	32.6 $\pm$ 2.4	9.5 $\pm$ 0.3	
	ATM <sup>KD</sup>	0.05% DMSO	65.6 $\pm$ 3.2	26.7 $\pm$ 2.5	7.7 $\pm$ 0.7	ns
		5 $\mu$ M 360A	61.9 $\pm$ 0.5	28.3 $\pm$ 0.3	9.8 $\pm$ 0.8	
EBV-lymphocytes	Normal	0.05% DMSO	48.8 $\pm$ 4.0	43.5 $\pm$ 3.5	7.7 $\pm$ 0.5	0.017
		5 $\mu$ M 360A	30.4 $\pm$ 0.7	63.3 $\pm$ 0.6	6.3 $\pm$ 1.3	
	AT	0.05% DMSO	62.5 $\pm$ 1.4	26 $\pm$ 1.4	11.5 $\pm$ 2.8	ns
		5 $\mu$ M 360A	69.9 $\pm$ 0.6	18.8 $\pm$ 0.9	11.3 $\pm$ 0.3	
SV40-fibroblasts	Normal	0.05% DMSO	49.7 $\pm$ 4.8	33.9 $\pm$ 3.4	16.4 $\pm$ 1.4	ns
		5 $\mu$ M 360A	44.6 $\pm$ 3.5	36.4 $\pm$ 1.7	19 $\pm$ 1.7	
	AT	0.05% DMSO	36.3 $\pm$ 4.3	40.3 $\pm$ 2.4	23.4 $\pm$ 6.8	ns
		5 $\mu$ M 360A	41.2 $\pm$ 8.6	37.8 $\pm$ 3.7	21 $\pm$ 4.9	

<sup>a</sup>Percentages of cells in different phases of the cell cycle are expressed with respect to the total number of viable cells. Means and standard deviations of two independent experiments are shown.

<sup>b</sup>For each cell line, the cell cycle distribution of 360A-treated cells was compared with that of DMSO controls by performing chi-square ( $\chi^2$ ) analysis on mean values. ns: non significant.

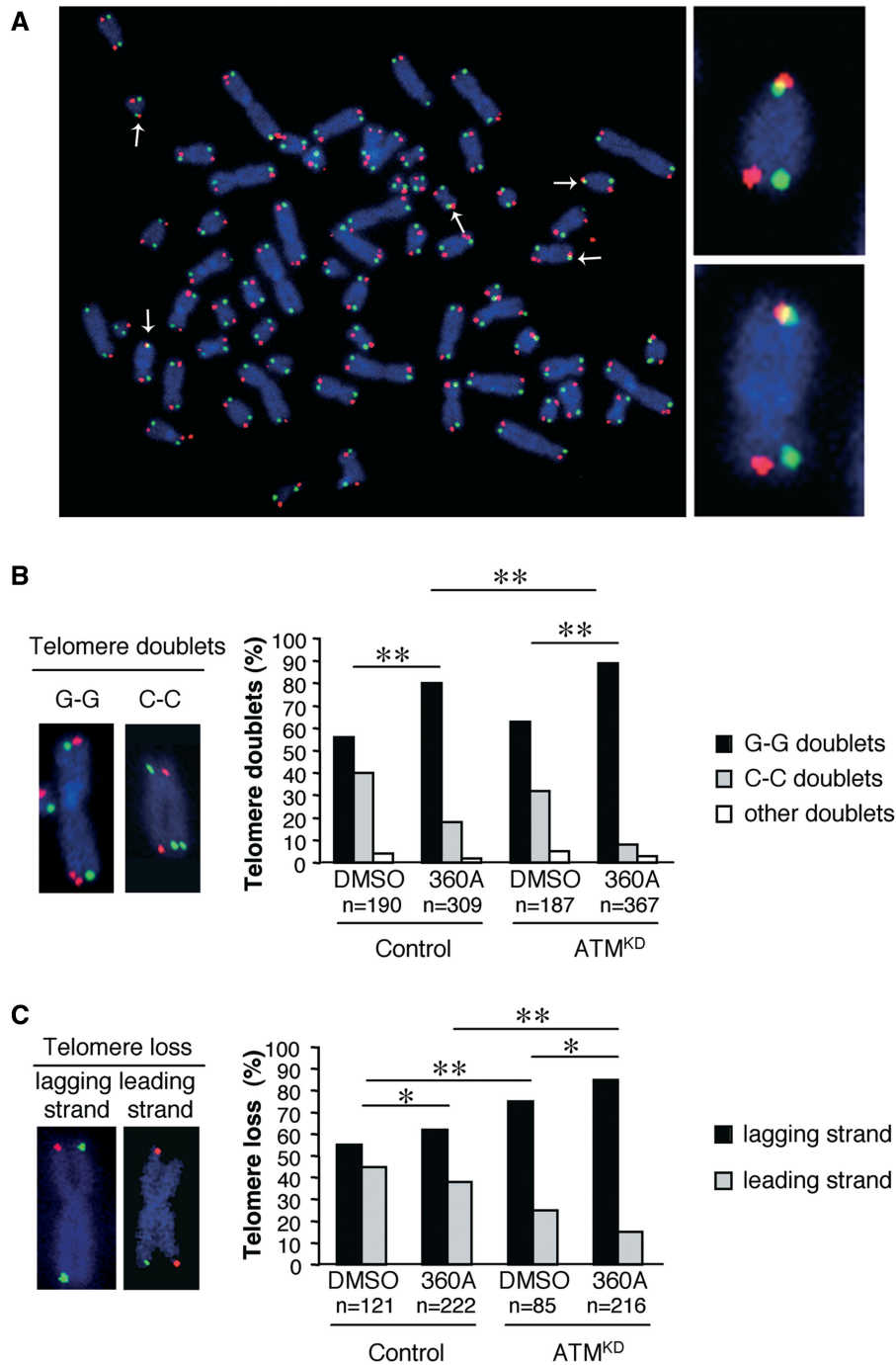


**Figure 4.** Respective involvement of lagging and leading telomeres in telomere aberrations induced by 360A revealed by CO-FISH in ATM<sup>KD</sup> and control HeLa cells. CO-FISH was performed on metaphases of ATM<sup>KD</sup> and control HeLa cells treated with 5  $\mu$ M 360A for 8 days (or 0.05% DMSO). Lagging strand telomeres are labeled in red and leading strand telomeres in green. (A) Example of CO-FISH analysis from metaphase spreads of HeLa cells treated with 360A for 8 days showing that sister chromatid fusions involved telomeres of the two chromatids (white arrows and enlarged views) and not telomere-DNA double-strand break fusions. (B) Respective percentages of telomere doublets containing two lagging strand telomeres (G-G doublets) or two leading strand telomeres (C-C doublets) or both lagging and leading strand telomeres (others doublets) in ATM<sup>KD</sup> and control HeLa cells. *n* = total number of telomere doublets analyzed. Examples of telomere doublets are shown on the left. Chi-square analysis was performed to detect differences in the repartition of telomere doublets containing two G-G, two C-C or other doublets between the different conditions (\*\**P* < 0.001). (C) Percentages of single telomere loss affecting the lagging or the leading strand in ATM<sup>KD</sup> and control HeLa cells. *n* = total number of telomere loss analyzed. Examples of missing lagging or leading strand telomeres are shown on the left. Chi-square analysis was performed to detect differences in the repartition of missing lagging or leading strand telomeres between the different conditions (\**P* < 0.05; \*\**P* < 0.001).



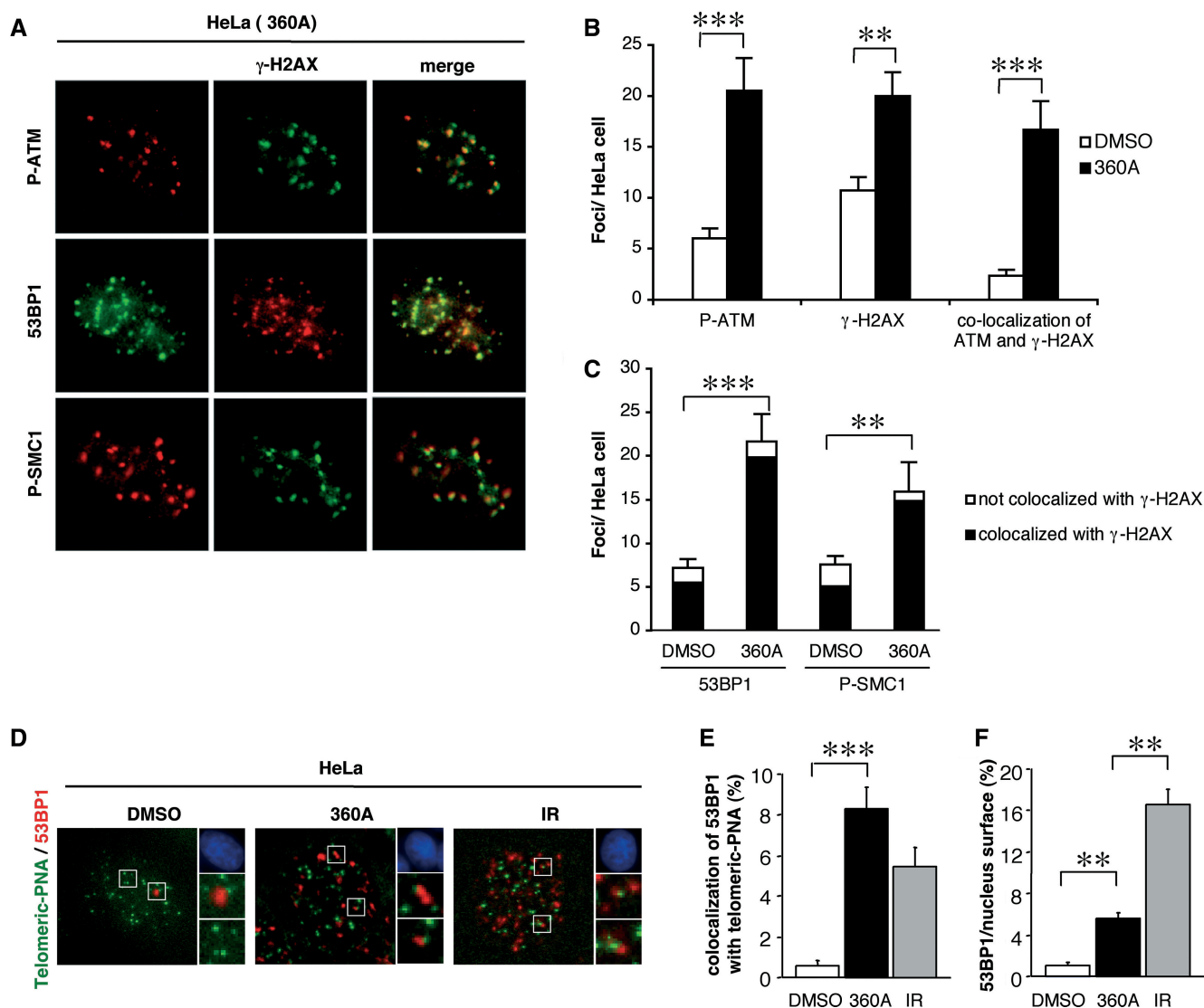


**Figure 5.** 360A induces DNA damage signaling. (A–C) 53BP1 and phosphorylated forms (P-) of ATM and SMC1 form foci that co-localized with  $\gamma$ -H2AX following 360A treatment in HeLa cells. HeLa cells were treated with 5  $\mu$ M 360A (or 0.05% DMSO as control) for 7 days, fixed and costained with anti- $\gamma$ -H2AX and specific antibodies of 53BP1, P-ATM and P-SMC1. Typical images of 360A-treated HeLa cells exhibited colocalizations between foci of  $\gamma$ -H2AX and DNA repair factors are shown in (A). Histograms (B) show the numbers of P-ATM,  $\gamma$ -H2AX foci and of their colocalization per cell calculated from at least 50 randomly chosen cells for each condition  $\pm$  SE (\*\*\*) indicate a *t*-test *P*-value  $< 0.0001$  and \*\**P*  $< 0.005$ ). (C) Colocalizations were quantified by scoring the number of 53BP1 and P-SMC1 foci colocalized or not with  $\gamma$ -H2AX foci in at least 50 randomly chosen cells per condition (\*\*\*) *P*  $< 0.0001$  and \*\**P*  $< 0.005$ ). (D–F) Colocalization of telomeric-PNA signals (green, in D) and 53BP1 foci (red, in D) in HeLa cells treated with 5  $\mu$ M 360A (or 0.05% DMSO) for 7 days or exposed to 2 Gy-irradiation (IR) and collected 1 h after irradiation. (D) Colocalization was appreciated on merge images shown on the left for the three conditions. Each image was obtained from a maximum projection of a Z-stack of 15 images, which were previously subjected to 2D deconvolution using the Metamorph software (Universal imaging corp.). Nuclei stained with DAPI (blue) and enlarged views of colocalized foci from the merged image are shown on the right. Percentage of 53BP1 signal colocalized with telomeric PNA signal (E) and percentages of nucleus surface occupied by 53BP1 foci (F) in the different conditions were calculated with colocalization module of the Metamorph software (\*\**P*  $< 0.001$ ; \*\*\**P*  $< 0.0001$ ).

$\gamma$ -H2AX (Figure 5A and C), consistently with the well-known role of  $\gamma$ -H2AX in the recruitment of DNA repair and checkpoint proteins at DNA damage sites (42).

We then investigated the localization of these DNA damage foci by immunostaining of 53BP1 followed by hybridization with a telomere-specific fluorescent PNA probe (Figure 5D and E). Colocalization of 53BP1 with PNA signals significantly increased 14 times in 360A-treated cells in comparison to DMSO controls

(8.3% versus 0.6%; Figure 5D and E). Since we found only around 5% of colocalization in 2 Gy-irradiated HeLa cells that had three times more 53BP1 foci than 360A-treated cells (Figure 5F), increase in overlapping between 53BP1 and PNA signals in 360A-treated cells cannot be the simple consequence of increased area of 53BP1 foci. Therefore, our results indicate that 360A induced a DNA damage signaling at telomeres similar to telomere dysfunction-induced foci (TIFs) (10,43).

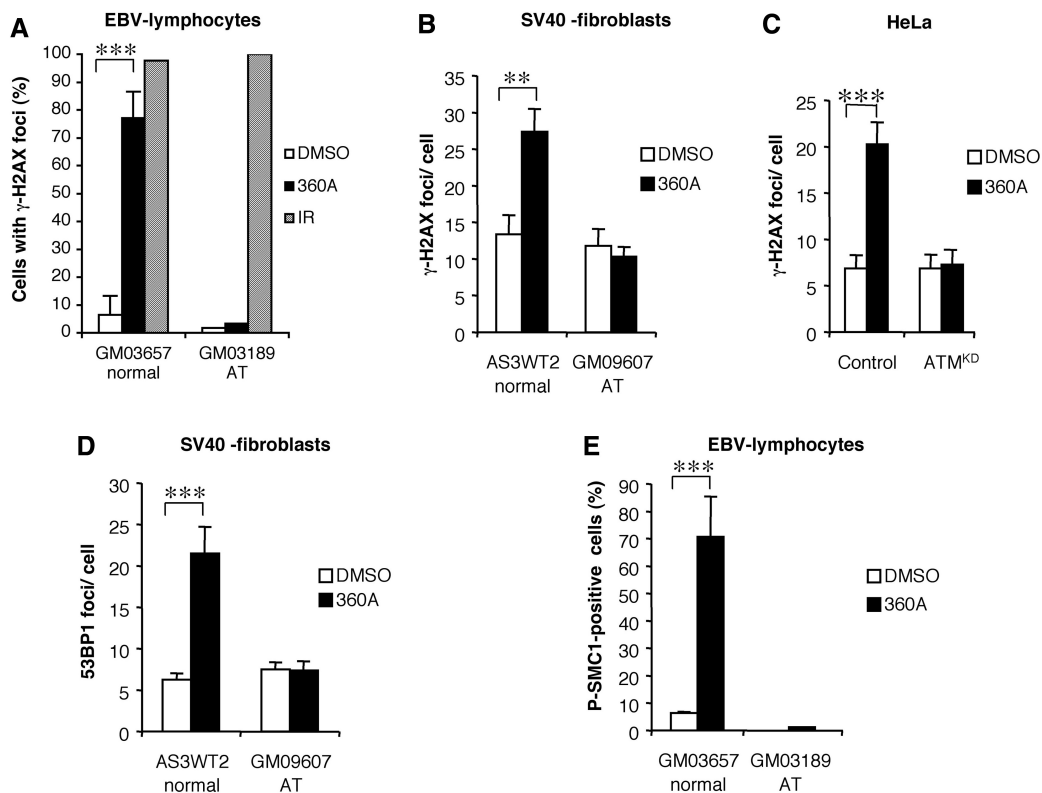


**Figure 6.** ATM is required for 360A-induced DNA damage signaling. (A) Percentage of cells with  $\gamma$ -H2AX foci in normal (GM03657) and AT (GM03189) EBV-lymphocyte cell lines treated with 5  $\mu$ M 360A or 0.05% DMSO for 7 days or exposed to 5-Gy IR as positive controls, then fixed and stained with anti- $\gamma$ -H2AX antibodies ( $***P < 0.0001$ ,  $n > 100$ ). (B, C) Number of  $\gamma$ -H2AX foci per cell in normal (AS3WT2) and AT (GM09607) SV40-fibroblasts (B) and in ATM<sup>KD</sup> and control HeLa cells (C) treated as described in (A) ( $**P < 0.001$ ;  $***P < 0.0001$ ;  $n \geq 50$ ). (D) Number of 53BP1 foci per cell in normal (AS3WT2) and AT (GM09607) SV40-fibroblasts treated as described in (A) ( $***P < 0.0001$ ,  $n = 50$ ). (E) Percentage of cells with phospho-SMC1 foci in normal (GM03657) and AT (GM03189) EBV-lymphocytes treated as described in (A) and immunostained with anti-phospho-SMC1 antibodies ( $***P = 0.0002$ ,  $n > 100$ ).

However, we showed that most of 53BP1 signals did not colocalize with that of PNA in 360A-treated cells. This could indicate that 360A induced other DNA damages at interstitial sites. Alternatively, some 360A-induced DNA damage foci may be localized at chromosome ends lacking telomeric repeats as suggested above by the elevated frequencies of telomere loss evidenced by FISH analysis in 360A-treated cultures.

Interestingly, 360A induced  $\gamma$ -H2AX, 53BP1 and SMC1 nuclear foci in ATM-proficient controls, but not in ATM-deficient cell lines and ATM<sup>KD</sup> HeLa cells (Figure 6). We verified that ionizing radiation induced the formation of  $\gamma$ -H2AX foci in ATM-deficient cells (Figure 6A and data not shown) indicating, as previously shown (42), that radio-induced DNA damages trigger H2AX phosphorylation in ATM-deficient cells through alternative pathways, for example involving the ATR kinase. Therefore, the lack of induction of  $\gamma$ -H2AX foci in 360A-treated ATM-deficient cells indicates the predominant role of ATM in the signaling of the DNA damages induced by the G-quadruplex ligand emphasizing their specificity compared to DSB-inducing treatments such as ionizing radiation that are able to activate  $\gamma$ -H2AX foci by alternative pathways involving ATR or DNA-PK (44,45).

## DISCUSSION

We showed here that loss of ATM function sensitized immortalized cell lines to a broad spectrum of telomere aberrations specifically induced by the G-quadruplex ligand 360A. The increase in telomere instability that we observed in 360A-treated ATM-deficient cells was not related to defect in cell cycle checkpoint or apoptosis induction but evidenced a direct role for ATM in preventing inappropriate DNA repair at dysfunctional telomeres.

### 360A induces a broad spectrum of specific telomere aberrations

The G-quadruplex ligand induced dicentric chromosomes, which are due to chromosome fusions in G1 or early S phases. We showed that these dicentric chromosomes specifically involved telomere fusions suggesting that they resulted from NHEJ (nonhomologous end joining) activation at dysfunctional telomeres (46) (Figure 7A). We also showed that 360A induced many telomere aberrations that have not been reported to date for other G-quadruplex ligands. This is the case of TDM that we found particularly in 360A-treated ATM-deficient cells. TDM have been proposed to result from

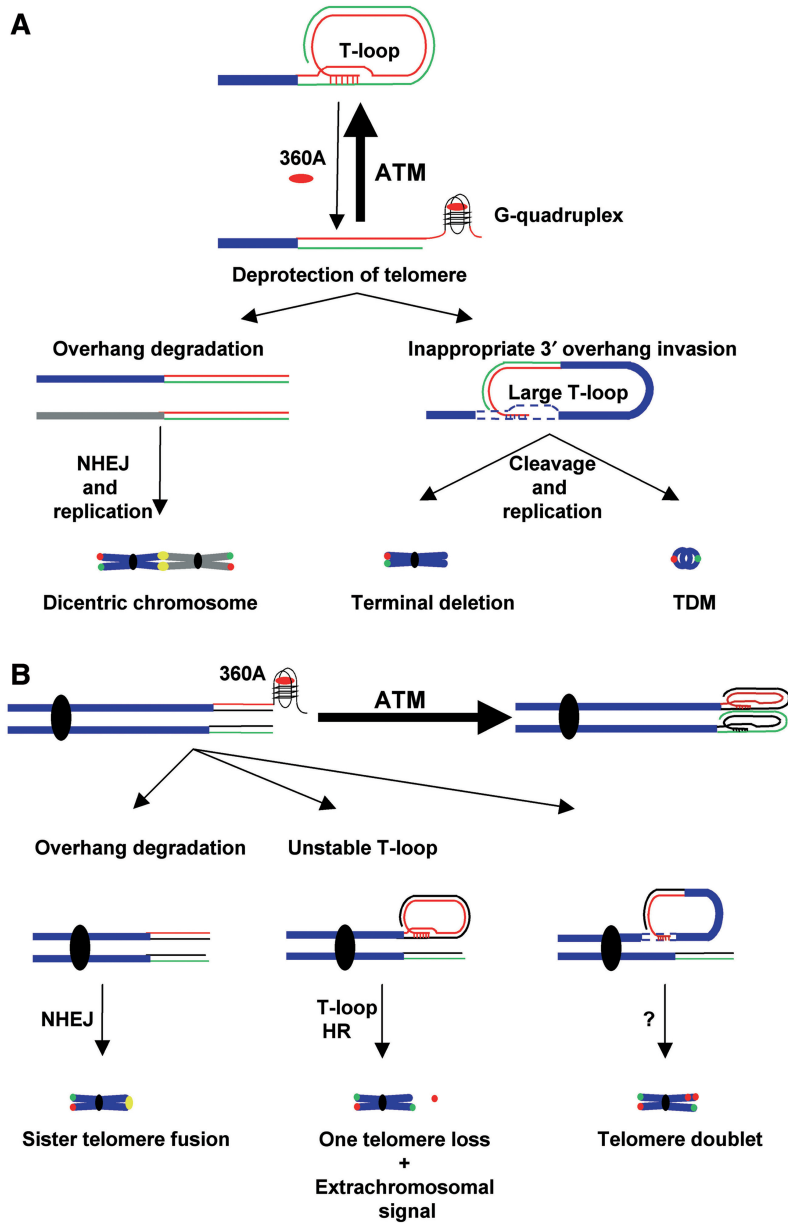


**Figure 7.** Model for 360A-induced telomere aberrations and the role of ATM in telomere stability. **(A)** 360A destabilizes telomere T-loops in G1 or early S by inducing or stabilizing G-quadruplexes at G-overhangs leading either to overhang degradation, or to inappropriate strand-invasion into interstitial telomere-related sequences in *cis* forming a large T-loop. In the first case, blunt-ended telomeres of distinct chromosomes can be fused by NHEJ, forming characteristic dicentric chromosomes at metaphase containing parental telomere strands at the fusion points (in yellow) (46). In the second case, which could be favored by 360A-induced G-quadruplexes at interstitial sites, recombination between telomere and interstitial sequences generates at metaphase a terminally deleted chromosome and a TDM corresponding to the large T-loop (37). **(B)** G-quadruplex formation at parental G-overhang prevents formation of a stable and protected telomere structure in late S and G2. This could lead either to overhang degradation, unstable T-loop formation or inappropriate overhang-invasion into interstitial sequences in *cis*. In the first case, blunt-ended telomere of the lagging strand can be fused by NHEJ with sister chromatid before generation of the leading strand G-overhang (alternatively leading strand telomere G-overhang could be degraded as a consequence of G-quadruplex formation) producing a metaphase chromosome with telomere sister fusion (in yellow). In the second case, unstable T-loop could undergo T-loop HR (47), which would result at metaphase in a chromosome lacking its lagging strand telomere and an extra chromosome signal containing parental telomere G-strands (*in cis*). In the third case, recombination between lagging strand chromosomes and interstitial sequences in *cis* produces telomere doublets made of two signals of the parental G strand (in red) separated by interstitial DNA sequences, although the precise mechanism involved is unknown. ATM could attenuate telomere instability by insuring the reformation of stable and protected structures at destabilized telomeres and after replication through its participation in the process of generation of T-loop structures. Parental G strands are in red, parental C strands in green and neosynthesized strands in black. Centromeres are represented as black ellipses.

homologous recombination (HR) between a dysfunctional telomere and interstitial DNA in *cis* forming a large T-loop containing nontelomeric DNA arrays (37). Subsequent cleavages, followed by replication, result in a TDM, a circular product containing two telomere signals (but no centromeric sequence) corresponding to the large T-loop and a terminally deleted chromosome lacking telomeres (37) (Figure 7A). At least some of the terminally deleted chromosomes found in treated cells may have thus been generated as a consequence of telomere destabilization.

Detection of both dicentric chromosomes and TDM indicates that 360A can destabilize telomeres in G1 or early S. But, one important finding of this study is that 360A mainly induced telomere aberrations that occurred during or after telomere replication (i.e. sister chromatid telomere fusions, loss of one telomere and telomere doublets), which highly suggests that 360A impedes reformation of a protected structure at telomeres at this step of the cell cycle.

Sister chromatid telomere fusions have been shown to be due to NHEJ (46) (Figure 7B). Their increase in 360A-treated cells suggests that 360A can act at both the lagging and the leading strand telomeres. However, one other important finding of the present study is the demonstration that the lagging strand telomeres were more frequently lost or involved in telomere doublets than the leading strand telomeres, particularly in 360A-treated ATM-deficient cells. This demonstrates that these types of recombination resulted from a specific telomere targeting by the compound. Metaphasic chromosomes lacking one telomere may have been generated by a process known as T-loop HR (47), in which the T-loop becomes a substrate for Holliday junction resolvases resulting in the deletion of a T-loop-sized segment (Figure 7B). This is consistent with the detection of extrachromosomal telomere signals formed principally with lagging strand telomeres in 360A-treated cells. Telomere doublets have been previously described in ATM-deficient mouse cell lines (13) and at low frequency in human cells (13,48). We demonstrated that their formation in 360A-treated cells involved, for most of them, only one chromatid, but no chromatid exchange and no further sequence duplication. Telomere doublets induced by the G-quadruplex ligand appear thus to originate principally from recombination between lagging strand telomeres and nontelomeric sequences in *cis*. We therefore propose that they derived from improper T-loop formation as proposed above for TDM, although the exact mechanisms remain to be elucidated (Figure 7B).

Moreover, preferential involvement of the lagging strand telomeres in 360A-induced recombination indicates the preferential targeting by the compound of the parental telomere G-strands (allowing the replication of the lagging strand telomeres), which is consistent with the putative mode of action of 360A through G-quadruplex formation and/or stabilization suggested by its high *in vitro* specificity and affinity for these structures (24,25). Furthermore, all the types of telomere recombination induced by 360A that we described here are also in agreement with the targeting by 360A of the

G-overhang preventing the formation of a stable T-loop, as proposed previously from *in vitro* binding assay on genomic DNA (25). Lower involvement of the newly synthesized G-strands (of the leading telomere) in recombinations may reflect lower accessibility to the compound of their G-overhangs, which contrary to that of the lagging strands absolutely require the action of a 5'-3' exonuclease to be generated (49,50).

We showed that 360A triggered DNA damage signaling outside telomeres that could be indicative of the formation of G-quadruplex structures at interstitial sites, as proposed previously (25,51). This is sustained by the need of functional ATM for this signaling to occur indicating the particularity of these DNA damages. The question of the importance of these interstitial DNA damages for the cellular effects induced by 360A remained asked. However, the telomere targeting by the G-quadruplex ligand is probably the main cause of cell death, since: (i) we did not detect by the methods used a significant level of genetic instability that did not involve telomeres in ATM-proficient, as well as in ATM-deficient cell lines, and (ii) the strong level of telomere instability and the frequent detection of anaphase bridges [data not shown; (24)] observed in treated cells are well consistent with the induction of mitotic catastrophe after few rounds of replication. This is further sustained by the rarity of duplicated telomere doublets on sister chromatids, confirming that the cells did not enter a second cycle of division after induction of telomere recombination regardless their ATM status. However, participation of interstitial DNA damages in telomere recombination could not be excluded. This is suggested particularly in case of TDM and telomere doublets, which are likely due to telomere recombination in *cis* with interstitial sequences as proposed above.

#### **ATM prevents activation of inappropriate DNA repair at 360A-induced dysfunctional telomeres**

We showed that ATM defect significantly and specifically increased telomere aberrations induced by 360A in three different cell contexts and that this was not related to impaired cell cycle checkpoints and apoptosis induction suggesting that ATM has a more direct role to protect telomeres. We showed that most of telomere aberrations induced by 360A, and significantly increased in ATM-deficient cells, resulted from the lack (telomere sister fusion), improper (telomere doublets) or unstable (single-strand telomere loss) formation of protected telomere structures during or after replication (Figure 7B). ATM has been shown to be recruited at telomere at every G2-M phase of the cell cycle and proposed to be needed for recruiting the HR machinery, which could promote T-loop formation (16,17). Our results give thus another indication that ATM has a role at telomeres at this step of the cell cycle, which supports the hypothesis that ATM participates to the formation of a stable and protected telomere structure. ATM could thus reduce telomere aberrations in 360A-treated cells by allowing the correct formation of a stable T-loop at destabilized telomeres preventing thus activation

of inappropriate DNA repair. Increases in dicentric chromosomes and TDM in 360A-treated ATM-deficient cells suggest that ATM may be also needed to reform a protected structure at telomeres destabilized by 360A at earlier phase of the cell cycle (Figure 7A).

Importantly, we found that 360A induced the formation of TIFs, similar—but at reduced quantitative levels—to that caused by telomere deprotection at cell senescence or resulting from TRF2 inhibition (10,43), which roles are still not clearly defined. The lack of TIF in ATM-deficient cells treated by 360A clearly demonstrates that TIFs are dispensable or not involved in the activation by the G-quadruplex-ligand of inappropriate DNA repair at dysfunctional telomeres. Rather, they may be directly involved in the protective role of ATM at telomeres.

To conclude, we showed that the G-quadruplex ligand 360A induced a large spectrum of specific telomere damages probably through the induction and/or stabilization of G-quadruplex at telomere overhangs preventing correct reformation of a stable T-loop structure. ATM appears to have a direct protective role against activation of inappropriate DNA repair mechanisms at dysfunctional telomeres, distinct from its roles in checkpoint activation and apoptosis induction, and which could be related to its possible participation in the process of T-loop formation.

## SUPPLEMENTARY DATA

Supplementary Data are available at NAR Online.

## ACKNOWLEDGEMENTS

The authors thank Patrick Mailliet (Aventis Pharma) and members of LRP for helpful discussions. Funding to pay the Open Access publication charges for this article was provided by Commissariat à l'Énergie Atomique.

*Conflict of interest statement.* None declared.

## REFERENCES

- de Lange, T. (2005) Shelterin: the protein complex that shapes and safeguards human telomeres. *Genes Dev.*, **19**, 2100–2110.
- Griffith, J.D., Comeau, L., Rosenfield, S., Stansel, R.M., Bianchi, A., Moss, H. and de Lange, T. (1999) Mammalian telomeres end in a large duplex loop. *Cell*, **97**, 503–514.
- Pandita, T.K. (2002) ATM function and telomere stability. *Oncogene*, **21**, 611–618.
- Shiloh, Y. (2003) ATM and related protein kinases: safeguarding genome integrity. *Nat. Rev. Cancer*, **3**, 155–168.
- Hurley, P.J. and Bunz, F. (2007) ATM and ATR: components of an integrated circuit. *Cell Cycle*, **6**, 414–417.
- Pandita, T.K., Lieberman, H.B., Lim, D.S., Dhar, S., Zheng, W., Taya, Y. and Kastan, M.B. (2000) Ionizing radiation activates the ATM kinase throughout the cell cycle. *Oncogene*, **19**, 1386–1391.
- Bakkenist, C.J. and Kastan, M.B. (2003) DNA damage activates ATM through intermolecular autophosphorylation and dimer dissociation. *Nature*, **421**, 499–506.
- Lavin, M.F. and Kozlov, S. (2007) ATM activation and DNA damage response. *Cell Cycle*, **6**, 931–942.
- Herbig, U., Jobling, W.A., Chen, B.P., Chen, D.J. and Sedivy, J.M. (2004) Telomere shortening triggers senescence of human cells through a pathway involving ATM, p53, and p21(CIP1), but not p16(INK4a). *Mol. Cell*, **14**, 501–513.
- Takai, H., Smogorzewska, A. and de Lange, T. (2003) DNA damage foci at dysfunctional telomeres. *Curr. Biol.*, **13**, 1549–1556.
- Denchi, E.L. and de Lange, T. (2007) Protection of telomeres through independent control of ATM and ATR by TRF2 and POT1. *Nature*, **448**, 1068–1071.
- Smilenov, L.B., Morgan, S.E., Mellado, W., Sawant, S.G., Kastan, M.B. and Pandita, T.K. (1997) Influence of ATM function on telomere metabolism. *Oncogene*, **15**, 2659–2665.
- Undarmaa, B., Kodama, S., Suzuki, K., Niwa, O. and Watanabe, M. (2004) X-ray-induced telomeric instability in Atm-deficient mouse cells. *Biochem. Biophys. Res. Commun.*, **315**, 51–58.
- Smilenov, L.B., Dhar, S. and Pandita, T.K. (1999) Altered telomere nuclear matrix interactions and nucleosomal periodicity in ataxia telangiectasia cells before and after ionizing radiation treatment. *Mol. Cell Biol.*, **19**, 6963–6971.
- Scherthan, H., Jerratsch, M., Dhar, S., Wang, Y.A., Goff, S.P. and Pandita, T.K. (2000) Meiotic telomere distribution and Sertoli cell nuclear architecture are altered in Atm- and Atm-p53-deficient mice. *Mol. Cell Biol.*, **20**, 7773–7783.
- Verdun, R.E., Crabbe, L., Haggblom, C. and Karlseder, J. (2005) Functional human telomeres are recognized as DNA damage in G2 of the cell cycle. *Mol. Cell*, **20**, 551–561.
- Verdun, R.E. and Karlseder, J. (2006) The DNA damage machinery and homologous recombination pathway act consecutively to protect human telomeres. *Cell*, **127**, 709–720.
- Verdun, R.E. and Karlseder, J. (2007) Replication and protection of telomeres. *Nature*, **447**, 924–931.
- Wang, Y. and Patel, D.J. (1993) Solution structure of the human telomeric repeat d[AG3(T2AG3)3] G-tetraplex. *Structure*, **1**, 263–282.
- Parkinson, G.N., Lee, M.P. and Neidle, S. (2002) Crystal structure of parallel quadruplexes from human telomeric DNA. *Nature*, **417**, 876–880.
- Neidle, S. and Parkinson, G.N. (2003) The structure of telomeric DNA. *Curr. Opin. Struct. Biol.*, **13**, 275–283.
- Kelland, L. (2007) Targeting the limitless replicative potential of cancer: the telomerase/telomere pathway. *Clin. Cancer Res.*, **13**, 4960–4963.
- De Cian, A., Lacroix, L., Douarre, C., Temime-Smaali, N., Trentesaux, C., Riou, J.F. and Mergny, J.L. (2008) Targeting telomeres and telomerase. *Biochimie*, **90**, 131–155.
- Pennarun, G., Granotier, C., Gauthier, L.R., Gomez, D., Hoffschir, F., Mandine, E., Riou, J.F., Mergny, J.L., Mailliet, P. and Boussin, F.D. (2005) Apoptosis related to telomere instability and cell cycle alterations in human glioma cells treated by new highly selective G-quadruplex ligands. *Oncogene*, **24**, 2917–2928.
- Granotier, C., Pennarun, G., Riou, L., Hoffschir, F., Gauthier, L.R., De Cian, A., Gomez, D., Mandine, E., Riou, J.F., Mergny, J.L. *et al.* (2005) Preferential binding of a G-quadruplex ligand to human chromosome ends. *Nucleic Acids Res.*, **33**, 4182–4190.
- Biard, D.S., Despras, E., Sarasin, A. and Angulo, J.F. (2005) Development of new EBV-based vectors for stable expression of small interfering RNA to mimic human syndromes: application to NER gene silencing. *Mol. Cancer Res.*, **3**, 519–529.
- Biard, D.S. (2007) Untangling the relationships between DNA repair pathways by silencing more than 20 DNA repair genes in human stable clones. *Nucleic Acids Res.*, **35**, 3535–3550.
- Bertrand, P., Akhmedov, A.T., Delacote, F., Durrbach, A. and Lopez, B.S. (1999) Human POMp75 is identified as the pro-oncoprotein TLS/FUS: both POMp75 and POMp100 DNA homologous pairing activities are associated to cell proliferation. *Oncogene*, **18**, 4515–4521.
- Dutrillaux, B. and Couturier, J. (1981) *La Pratique de L'analyse Chromosomique*. Masson, Paris.
- Lansdorp, P.M., Verwoerd, N.P., van de Rijke, F.M., Dragowska, V., Little, M.T., Dirks, R.W., Raap, A.K. and Tanke, H.J. (1996) Heterogeneity in telomere length of human chromosomes. *Hum. Mol. Genet.*, **5**, 685–691.
- Pandita, T.K. and DeRubeis, D. (1995) Spontaneous amplification of interstitial telomeric bands in Chinese hamster ovary cells. *Cytogenet. Cell. Genet.*, **68**, 95–101.
- Goodwin, E. and Meyne, J. (1993) Strand-specific FISH reveals orientation of chromosome 18 alphoid DNA. *Cytogenet. Cell. Genet.*, **63**, 126–127.

33. Incles, C.M., Schultes, C.M., Kempfski, H., Koehler, H., Kelland, L.R. and Neidle, S. (2004) A G-quadruplex telomere targeting agent produces p16-associated senescence and chromosomal fusions in human prostate cancer cells. *Mol. Cancer Ther.*, **3**, 1201–1206.
34. Leonetti, C., Amodi, S., D'Angelo, C., Rizzo, A., Benassi, B., Antonelli, A., Elli, R., Stevens, M.F., D'Incalci, M., Zupi, G. *et al.* (2004) Biological activity of the G-quadruplex ligand RHPS4 (3,11-difluoro-6,8,13-trimethyl-8H-quinolo[4,3,2-k]acridinium methosulfate) is associated with telomere capping alteration. *Mol. Pharmacol.*, **66**, 1138–1146.
35. Hande, M.P., Balajee, A.S., Tchirkov, A., Wynshaw-Boris, A. and Lansdorp, P.M. (2001) Extra-chromosomal telomeric DNA in cells from Atm(-/-) mice and patients with ataxia-telangiectasia. *Hum. Mol. Genet.*, **10**, 519–528.
36. van Overbeek, M. and de Lange, T. (2006) Apollo, an Artemis-related nuclease, interacts with TRF2 and protects human telomeres in S phase. *Curr. Biol.*, **16**, 1295–1302.
37. Zhu, X.D., Niedernhofer, L., Kuster, B., Mann, M., Hoeijmakers, J.H. and de Lange, T. (2003) ERCC1/XPF removes the 3' overhang from uncapped telomeres and represses formation of telomeric DNA-containing double minute chromosomes. *Mol. Cell.*, **12**, 1489–1498.
38. Abraham, R.T. (2001) Cell cycle checkpoint signaling through the ATM and ATR kinases. *Genes Dev.*, **15**, 2177–2196.
39. Bailey, S.M., Brenneman, M.A. and Goodwin, E.H. (2004) Frequent recombination in telomeric DNA may extend the proliferative life of telomerase-negative cells. *Nucleic Acids Res.*, **32**, 3743–3751.
40. Rogakou, E.P., Pilch, D.R., Orr, A.H., Ivanova, V.S. and Bonner, W.M. (1998) DNA double-stranded breaks induce histone H2AX phosphorylation on serine 139. *J. Biol. Chem.*, **273**, 5858–5868.
41. Hao, L.Y., Strong, M.A. and Greider, C.W. (2004) Phosphorylation of H2AX at short telomeres in T cells and fibroblasts. *J. Biol. Chem.*, **279**, 45148–45154.
42. Fernandez-Capetillo, O., Lee, A., Nussenzweig, M. and Nussenzweig, A. (2004) H2AX: the histone guardian of the genome. *DNA Repair (Amst.)*, **3**, 959–967.
43. d'Adda di Fagagna, F., Reaper, P.M., Clay-Farrace, L., Fiegler, H., Carr, P., Von Zglinicki, T., Saretzki, G., Carter, N.P. and Jackson, S.P. (2003) A DNA damage checkpoint response in telomere-initiated senescence. *Nature*, **426**, 194–198.
44. Stiff, T., O'Driscoll, M., Rief, N., Iwabuchi, K., Lobrich, M. and Jeggo, P.A. (2004) ATM and DNA-PK function redundantly to phosphorylate H2AX after exposure to ionizing radiation. *Cancer Res.*, **64**, 2390–2396.
45. Ward, I.M. and Chen, J. (2001) Histone H2AX is phosphorylated in an ATR-dependent manner in response to replicational stress. *J. Biol. Chem.*, **276**, 47759–47762.
46. Smogorzewska, A., Karlseder, J., Holtgreve-Grez, H., Jauch, A. and de Lange, T. (2002) DNA ligase IV-dependent NHEJ of deprotected mammalian telomeres in G1 and G2. *Curr. Biol.*, **12**, 1635–1644.
47. Wang, R.C., Smogorzewska, A. and de Lange, T. (2004) Homologous recombination generates T-loop-sized deletions at human telomeres. *Cell*, **119**, 355–368.
48. Philippe, C., Coullin, P. and Bernheim, A. (1999) Double telomeric signals on single chromatids revealed by FISH and PRINS. *Ann. Genet.*, **42**, 202–209.
49. Olovnikov, A.M. (1973) A theory of marginotomy. The incomplete copying of template margin in enzymic synthesis of polynucleotides and biological significance of the phenomenon. *J. Theor. Biol.*, **41**, 181–190.
50. Makarov, V.L., Hirose, Y. and Langmore, J.P. (1997) Long G tails at both ends of human chromosomes suggest a C strand degradation mechanism for telomere shortening. *Cell*, **88**, 657–666.
51. Burge, S., Parkinson, G.N., Hazel, P., Todd, A.K. and Neidle, S. (2006) Quadruplex DNA: sequence, topology and structure. *Nucleic Acids Res.*, **34**, 5402–5415.